

Determination of the Photolysis Products of [FeFe]Hydrogenase Enzyme Model Systems using Ultrafast Multidimensional Infrared Spectroscopy

Andrew I. Stewart,[†] Joseph A. Wright,[‡] Gregory M. Greetham,[§] Spiridon Kaziannis,[†] Stefano Santabarbara,[†] Michael Towrie,[§] Anthony W. Parker,[§] Christopher J. Pickett,^{*,‡} and Neil T. Hunt^{*,†}

[†]Department of Physics, University of Strathclyde, SUPA, 107 Rottenrow East, Glasgow, U.K.,

[‡]School of Chemical Sciences, University of East Anglia, Norwich, U.K., and [§]Central Laser Facility, STFC Rutherford Appleton Laboratory, Didcot, Oxon, U.K.

Received June 28, 2010

Ultrafast transient 2D-IR (T-2D-IR) spectroscopy has been used to study the photolysis products of the [FeFe]hydrogenase enzyme model compound (μ -propanedithiolate) $\text{Fe}_2(\text{CO})_6$ in heptane solution following irradiation at ultraviolet wavelengths. Observation of coupling patterns between the vibrational modes of the photoproduct species formed alongside examination of the appearance time scales of these signals has uniquely enabled assignment of the photoproduct spectrum to a single pentacarbonyl species. Comparison of the vibrational relaxation rate of the photoproduct with that of the parent is consistent with the formation of a solvent adduct at the vacant coordination site, while anisotropy data in conjunction with density functional theory simulations indicates substitution in an axial rather than equatorial position. No firm evidence of additional short-lived intermediates is seen, indicating that the subsequent chemistry of these species is likely to be strongly defined by the nature of the first solvation shell.

Introduction

One of the most important questions facing modern scientific research is to determine the exact process by which chemical reactions occur. This applies not only to the mechanism of reaction; the well-defined steps by which a chemical process proceeds, but also to the structure and behavior of the transition states and intermediates that lie between these mechanistic stepping stones. Such a thorough understanding of chemical reaction processes will ultimately enhance our ability to control and exploit them in a variety of arenas.

One example where this understanding may be important to new technological developments is the hydrogenase enzymes, which catalyze the reversible activation of molecular hydrogen, and the synthesis and reactions of active site model compounds of these have attracted much interest. While the [NiFe]H enzymes have been extensively studied^{1–4} it is the [FeFe]H system that has been the focus of considerably more synthetic

model studies resulting from the structural similarity of the active site to complexes of the form (μ -SRS) $\text{Fe}_2(\text{CO})_6$.^{5–8} These models allow studies of the active site of the enzymes without the complication of the surrounding protein,^{9–11} and it has also been shown that such synthetic analogues are also capable of catalyzing the reduction of protons.⁵

One important facet of hydrogenase chemistry is the inhibition of catalysis by CO. Studies using irradiation of the CO-inhibited state at cryogenic temperatures have shown evidence for a structure identical to that of the oxidized form of the enzyme.¹² UV-FTIR studies of iron carbonyl sulfide, $\text{Fe}_2(\text{CO})_6(\mu\text{-S}_2)$ in a matrix showed that the two lowest energy transitions in the UV–visible region of the spectrum correspond to Fe–Fe bond activation at 450 nm, while higher energy absorptions ($285 < \lambda < 420$ nm) correspond to metal to ligand charge-transfer transitions and result in the loss of a carbonyl ligand.¹³ The role of CO loss in the enzyme

*To whom correspondence should be addressed. E-mail: nhunt@phys.strath.ac.uk.

- (1) Frey, M. *Struct. Bonding (Berlin)* **1998**, *90*, 98.
- (2) Fontecilla-Camps, J. C. *Coord. Chem. Rev.* **2005**, *249*, 1609.
- (3) de Lacey, A. L.; Fernandez, V. M.; Rousset, M. *Coord. Chem. Rev.* **2005**, *249*, 1596.
- (4) Frey, M. *ChemBioChem* **2002**, *3*, 153.
- (5) Liu, X. M.; Ibrahim, S. K.; Tard, C.; Pickett, C. J. *Coord. Chem. Rev.* **2005**, *249*, 1641.
- (6) Borg, S. J.; Tye, J. W.; Hall, M. B.; Best, S. P. *Inorg. Chem.* **2007**, *46*, 384.
- (7) Borg, S. J.; Behrsing, T.; Best, S. P.; Razavet, M.; Liu, X.; Pickett, C. J. *J. Am. Chem. Soc.* **2004**, *126*, 16988.

(8) Tard, C.; Liu, X. M.; Ibrahim, S. K.; Bruschi, M.; De Gioia, L.; Davies, S. C.; Yang, X.; Wang, L. S.; Sawers, G.; Pickett, C. J. *Nature* **2005**, *433*, 610.

(9) Bonner, G. M.; Ridley, A. R.; Ibrahim, S. K.; Pickett, C. J.; Hunt, N. T. *Faraday Discuss.* **2010**, *145*, 429.

(10) Stewart, A. I.; Clark, I. P.; Towrie, M.; Ibrahim, S.; Parker, A. W.; Pickett, C. J.; Hunt, N. T. *J. Phys. Chem. B* **2008**, *112*, 10023.

(11) Ridley, A. R.; Stewart, A. I.; Adamczyk, K.; Ghosh, H. N.; Kerkeni, B.; Guo, Z. X.; Nibbering, E. T. J.; Pickett, C. J.; Hunt, N. T. *Inorg. Chem.* **2008**, *47*, 7453.

(12) Chen, Z.; Lemon, B. J.; Huang, S.; Swartz, D. J.; Peters, J. W.; Bagley, K. A. *Biochemistry* **2002**, *41*, 2036.

(13) Silaghi-Dumitrescu, I.; Bitterwolf, T. E.; King, R. B. *J. Am. Chem. Soc.* **2006**, *128*, 5342.

mechanism makes the latter transition the most pertinent to this study, but, to date, the ultrafast dynamics of these species remains largely unexplored.

In a recent study using a combination of ultrafast UV_{pump}-IR_{probe} and UV pumped FTIR spectroscopies,¹¹ it was determined that irradiation of (μ -propanedithiolate)Fe₂(CO)₆ [**1**] in room temperature heptane solution at 350 nm resulted in a complex set of photoproduct vibrational modes consistent with the loss of a carbonyl ligand. Despite the use of Density Functional Theory (DFT) spectral simulations and the fact that alkane coordination to vacant sites of metal carbonyls following photolysis is well-known,^{14–17} it was impossible to determine whether these modes were due to a single species or a mixture of products including those with a vacant coordination site and a solvent adduct. Additional investigations of hydrogenase photochemistry using DFT methods have been reported¹⁸ and have suggested a most probable photoproduct structure, but this has yet to be confirmed spectroscopically and the role of the solvent was not considered explicitly. Raman spectroscopy has also been employed to assign the Raman active vibrational modes of a (μ -SRS)Fe₂(CO)₆-type molecule and steps were taken to determine the quantum yield for photolysis, but it was concluded that more work was required to identify the photoproducts.¹⁹

A solution to this problem lies in the technique of ultrafast transient 2D-IR (T-2D-IR) spectroscopy.^{20–22} 2D-IR methods are based upon a sequence of ultrafast infrared laser pulses and are analogous to the radio frequency pulse sequences used to obtain 2D-NMR spectra. In the case of 2D-IR, the radiation–matter interaction pathway is via vibrational rather than nuclear spin energy levels, and the experiments result in a molecular infrared response that is spread over two frequency axes allowing access to a significant amount of additional information in relation to 1D methods. Further, the time resolution of the infrared analogue is many orders of

magnitude higher than NMR methods. 2D-IR has been used to good effect in many applications including molecular structure^{23–31} and transition state determination,³² vibrational dynamics and solvent–solute interactions,^{33–42} and chemical exchange processes.^{43–45} The subject has been the topic of recent review articles,^{20,46–49} but the most pertinent advantage of 2D methods in this case is that peaks are observed in the off-diagonal region of the spectrum which identify the presence of vibrational coupling between infrared modes. As such, it is possible to identify and, if necessary, separate overlapping spectra to provide a definite analysis of complex spectra.⁵⁰

In the case of T-2D-IR methods, 2D-IR spectroscopy is employed as a time-delayed probe of a photochemical system allowing more detailed interrogation of the photoproducts.⁵¹ To date, it has allowed extraction of both photoproduct vibrational dynamics,^{51–53} excited state solvent–solute interaction dynamics,⁵⁴ and insights into the temporal evolution of the 2D-IR spectrum effectively in real-time.^{21,55,56}

In this article, we report a T-2D-IR experimental investigation of the photochemistry and dynamics of **1** in heptane solution. It has been shown that photolysis of **1** in a range of solvents leads to broadly similar photoproduct spectra but that alkane solvents have the advantage of producing significantly narrower linewidths and thus enable the maximum spectral resolution.¹¹ Through the presence in the T-2D-IR spectra of off-diagonal peaks

(14) Shilov, A. E.; Shul'pin, G. B. *Activation and Catalytic Reactions of Saturated Hydrocarbons in the presence of Metal Complexes*; Kluwer: The Netherlands, 2000.

(15) Hall, C.; Perutz, R. N. *Chem. Rev.* **1996**, *96*, 3125.
 (16) Bitterwolf, T. E. *J. Organomet. Chem.* **2004**, *689*, 3939.
 (17) Lian, T.; Bromberg, S. E.; Asplund, M. C.; Yang, H.; Harris, C. B. *J. Phys. Chem.* **1996**, *100*, 11994.
 (18) Bertini, L.; Greco, C.; de Gioia, L.; Fantucci, P. *J. Phys. Chem. A* **2009**, *113*, 5657.
 (19) Galinato, M. G. I.; Whaley, C. M.; Lehnert, N. *Inorg. Chem.* **2010**, *49*, 3201.
 (20) Bredenbeck, J.; Helbing, J.; Kolano, C.; Hamm, P. *ChemPhysChem* **2007**, *8*, 1747.
 (21) Kolano, C.; Helbing, J.; Kozinski, M.; Sander, W.; Hamm, P. *Nature* **2006**, *444*, 469.
 (22) Bredenbeck, J.; Helbing, J.; Hamm, P. *J. Chem. Phys.* **2004**, *121*, 5943.
 (23) Demirdoven, N.; Cheatum, C. M.; Chung, H. S.; Khalil, M.; Knoester, J.; Tokmakoff, A. *J. Am. Chem. Soc.* **2004**, *126*, 7981.
 (24) Cheatum, C. M.; Tokmakoff, A.; Knoester, J. *J. Chem. Phys.* **2004**, *120*, 8201.
 (25) Chung, H. S.; Khalil, M.; Tokmakoff, A. *Biophys. J.* **2004**, *86*, 526A.
 (26) Smith, A. W.; Cheatum, C. M.; Chung, H. S.; Demirdoven, N.; Khalil, M.; Knoester, J.; Tokmakoff, A. *Biophys. J.* **2004**, *86*, 619A.
 (27) Rubtsov, I. V.; Wang, J.; Hochstrasser, R. M. *J. Chem. Phys.* **2003**, *118*, 7733.
 (28) Hamm, P.; Lim, M.; De Grado, W. F.; Hochstrasser, R. M. *Proc. Natl. Acad. Sci. U.S.A.* **1999**, *96*, 2036.
 (29) Hamm, P.; Lim, M.; Hochstrasser, R. M. *J. Phys. Chem. B* **1998**, *102*, 6123.
 (30) Kim, Y. S.; Wang, J.; Hochstrasser, R. M. *J. Phys. Chem. B* **2005**, *109*, 7511.
 (31) Fang, C.; Senes, A.; Cristian, L.; De Grado, W. F.; Hochstrasser, R. M. *Proc. Natl. Acad. Sci. U.S.A.* **2006**, *103*, 16740.

(32) Cahoon, J. F.; Sawyer, K. R.; Schlegel, J. P.; Harris, C. B. *Science* **2008**, *319*, 1820.

(33) Khalil, M.; Demirdoven, N.; Tokmakoff, A. *J. Phys. Chem. A* **2003**, *107*, 5258.
 (34) Khalil, M.; Tokmakoff, A. *Chem. Phys.* **2001**, *266*, 213.
 (35) Okumura, K.; Tokmakoff, A.; Tanimura, Y. *Chem. Phys. Lett.* **1999**, *314*, 488.
 (36) Roberts, S. T.; Loparo, J. J.; Tokmakoff, A. *J. Chem. Phys.* **2006**, *125*, 084502.
 (37) Tokmakoff, A. *Science* **2007**, *317*, 54.
 (38) Fecko, C. J.; Loparo, J. J.; Roberts, S. T.; Tokmakoff, A. *J. Chem. Phys.* **2005**, *122*, 054506.
 (39) Steinel, T.; Asbury, J. B.; Corcelli, S. A.; Lawrence, C. P.; Skinner, J. L.; Fayer, M. D. *Chem. Phys. Lett.* **2004**, *386*, 295.
 (40) Asbury, J. B.; Steinel, T.; Kwak, K.; Corcelli, S. A.; Lawrence, C. P.; Skinner, J. L.; Fayer, M. D. *J. Chem. Phys.* **2004**, *121*, 12431.
 (41) Asbury, J. B.; Steinel, T.; Fayer, M. D. *J. Phys. Chem. B* **2004**, *108*, 6544.
 (42) Park, S.; Fayer, M. D. *Proc. Natl. Acad. Sci. U.S.A.* **2007**, *104*, 16731.
 (43) Woutersen, S.; Mu, Y.; Stock, G.; Hamm, P. *Chem. Phys.* **2001**, *266*, 137.
 (44) Kwak, K.; Zheng, J. R.; Cang, H.; Fayer, M. D. *J. Phys. Chem. B* **2006**, *110*, 19998.
 (45) Zheng, J. R.; Kwak, K.; Asbury, J. B.; Chen, X.; Piletic, I. R.; Fayer, M. D. *Science* **2005**, *309*, 1338.
 (46) Hochstrasser, R. M. *Proc. Natl. Acad. Sci. U.S.A.* **2007**, *104*, 14190.
 (47) Finkelstein, I. J.; Zheng, J. R.; Ishikawa, H.; Kim, S.; Kwak, K.; Fayer, M. D. *Phys. Chem. Chem. Phys.* **2007**, *9*, 1533.
 (48) Ganim, Z.; Chung, H. S.; Smith, A. W.; Deflores, L. P.; Jones, K. C.; Tokmakoff, A. *Acc. Chem. Res.* **2008**, *41*, 432.
 (49) Hunt, N. T. *Chem. Soc. Rev.* **2009**, *38*, 1837.
 (50) Asbury, J. B.; Steinel, T.; Fayer, M. D. *Chem. Phys. Lett.* **2003**, *381*, 139.
 (51) Kania, R.; Stewart, A. I.; Clark, I. P.; Greetham, G. M.; Parker, A. W.; Towrie, M.; Hunt, N. T. *Phys. Chem. Chem. Phys.* **2010**, *12*, 1051.
 (52) Baiz, C. R.; McCanne, R.; Nee, M. J.; Kubarych, K. J. *J. Phys. Chem. A* **2009**, *113*, 8907–8916.
 (53) Baiz, C. R.; McCanne, R.; Kubarych, K. J. *J. Am. Chem. Soc.* **2009**, *131*, 13590.
 (54) Bredenbeck, J.; Helbing, J.; Hamm, P. *J. Am. Chem. Soc.* **2004**, *126*, 990.
 (55) Kolano, C.; Helbing, J.; Kozinski, M.; Sander, W.; Hamm, P. *Nature* **2006**, *444*, 469.
 (56) Bredenbeck, J.; Helbing, J.; Behrendt, R.; Renner, C.; Moroder, L.; Wachtveitl, J.; Hamm, P. *J. Phys. Chem. B* **2003**, *107*, 8654.

linking photoproduct vibrational modes we were able to identify and definitively assign the spectra observed, and, through the time resolution of the T-2D-IR technique, we were able to investigate the possible formation of short-lived transient intermediate species. Insights into the molecular structure of the photoproduct species and the vibrational relaxation dynamics were also obtained.

Experimental Section

The T-2D-IR methodology employed here has been discussed elsewhere.⁵¹ Briefly, the T-2D-IR spectra were obtained using the ULTRA spectrometer and employed the frequency domain double resonance method for collection of 2D-IR spectra.^{28,29} In this case, the output of two synchronized Ti:sapphire regeneratively amplified lasers (40 fs and 2 ps pulse duration respectively; pulse repetition rate: 10 kHz) were used to pump two mid-infrared optical parametric amplifiers (OPA). The narrow bandwidth ($10\text{--}12\text{ cm}^{-1}$) infrared pump (IR_{pump}) pulse used for 2D-IR spectroscopy was produced by the OPA pumped by the 800 nm pulses generated by the ps pulse duration regenerative amplifier, while the broadband (400 cm^{-1}) probe (IR_{probe}) pulses were derived from the fs pulse-duration amplifier-OPA pair. A second OPA, employing second and fourth harmonic generation methods and pumped by a portion of the output from the fs pulse duration regenerative amplifier produced the 350 nm wavelength pulses that were used as a photolysis (UV_{pump}) pulse for TRIR and T-2D-IR spectroscopy. The data collection method employed was slightly different to that used in previous work; by chopping the UV_{pump} and IR_{pump} pulse trains at one-quarter and one-half of the laser repetition rate, respectively, it was possible to obtain time-resolved infrared ($\text{UV}_{\text{pump}}\text{-IR}_{\text{probe}}$), 2D-IR ($\text{IR}_{\text{pump}}\text{-IR}_{\text{probe}}$), and T-2D-IR ($\text{UV}_{\text{pump}}\text{-IR}_{\text{pump}}\text{-IR}_{\text{probe}}$) spectra along with a background signal (no pump pulses present) in four consecutive laser shots.²² Averaging over many such groups of laser pulses then allowed acquisition of each of these three data sets effectively simultaneously. Dynamical information was extracted by varying the time delays between the $\text{UV}_{\text{pump}}\text{-IR}_{\text{pump}}$ and $\text{IR}_{\text{pump}}\text{-IR}_{\text{probe}}$ pump pairs, which were controlled by optical delay lines. In the former case, this time delay allows access to information pertaining to photochemical evolution of the system, while the latter provides information on vibrational and rotational dynamics of each of the components.

The compound **1** used in this work was prepared using established methods,⁵ while the heptane (HPLC grade) was obtained from Sigma-Aldrich and used without further purification. All solvents were deoxygenated via purging with dry nitrogen prior to use. The samples were held between two CaF_2 windows separated by a PTFE spacer (100 μm thickness) and the concentration adjusted to give an optical density in the carbonyl stretching region of the infrared of around 0.4, which equated to an approximate concentration of 1 mM. UV-vis absorption experiments confirmed that the OD at 350 nm of these solutions was also close to 0.4 under these conditions. To ensure that the sample volume was refreshed between laser pulses, a rapid-flow system was employed to prevent spectral signatures due to multiple pumping of photoproduct species contaminating the data. Furthermore, the infrared and ultraviolet pulse intensities were adjusted to a level below that where the lineshapes ceased to show laser power dependence; the pulse energy for the UV_{pump} beam (350 nm) was in the region of $2\ \mu\text{J}$ while that of the IR_{pump} beam was around $1\ \mu\text{J}$. In all experiments described below, the polarization directions of the UV_{pump} and IR_{probe} pulses were parallel, with that of the IR_{pump} variable to allow extraction of vibrational relaxation dynamics and anisotropy parameters.

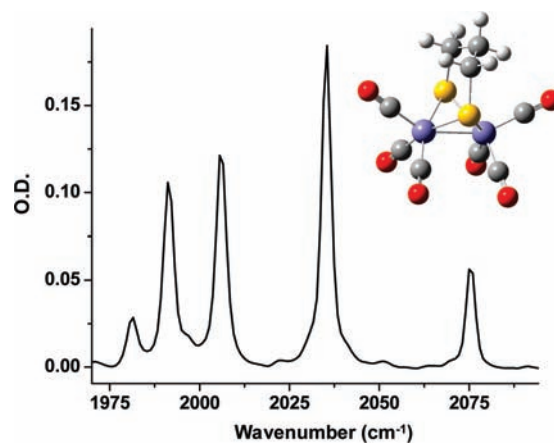


Figure 1. Infrared spectrum of a solution of **1** in heptane in the carbonyl stretching region of the mid-infrared. The response of the heptane solvent in this region is minimal but has been subtracted for clarity. Inset shows the molecular structure of **1**; Fe atoms are indicated by the color purple; S, yellow; C, gray; O, red and H, white.

All DFT calculations were carried out using the Gaussian 03 package.⁵⁷ Structural optimizations were performed prior to simulation of 1D infrared spectra. The calculations were performed on gas phase molecules using the B3LYP functional⁵⁸ and the LanL2DZ basis set. The latter employs the Dunning/Huzinaga valence double- ζ D95 V⁵⁹ basis set for first row atoms and the Los Alamos Effective Core Potential plus DZ on atoms from Na–Bi.^{60–62} No scaling or correction factors were applied.

Results and Discussion

The structure of compound **1** is shown in Figure 1 alongside the infrared absorption spectrum of a solution of **1** in heptane in the carbonyl stretching region of the mid-infrared region near 2000 cm^{-1} . The infrared spectroscopy, vibrational dynamics, and solution-phase structure of **1** were determined using 2D-IR methods previously and have been reported elsewhere but briefly, the spectrum consists of four intense transitions located at 2075, 2035, 2006, and 1991 cm^{-1} and a weaker transition located at 1982 cm^{-1} which are assignable to group vibrations of the $\text{Fe}_2(\text{CO})_6$ moiety.¹⁰

As mentioned above, time-resolved infrared spectroscopy (TRIR) studies have revealed that photolysis of **1** in heptane

(57) Frisch, M. J.; Trucks, G. W.; Schlegel, H. B.; Scuseria, G. E.; Robb, M. A.; Cheeseman, J. R.; Jr., J. A. M.; Vreven, T.; Kudin, K. N.; Burant, J. C.; Millam, J. M.; Iyengar, S. S.; Tomasi, J.; Barone, V.; Mennucci, B.; Cossi, M.; Scalmani, G.; Rega, N.; Petersson, G. A.; Nakatsuji, H.; Hada, M.; Ehara, M.; Toyota, K.; Fukuda, R.; Hasegawa, J.; Ishida, M.; Nakajima, T.; Honda, Y.; Kitao, O.; Nakai, H.; Klene, M.; Li, X.; Knox, J. E.; Hratchian, H. P.; Cross, J. B.; Bakken, V.; Adamo, C.; Jaramillo, J.; Gomperts, R.; Stratmann, R. E.; Yazyev, O.; Austin, A. J.; Cammi, R.; Pomelli, C.; Ochterski, J. W.; Ayala, P. Y.; Morokuma, K.; Voth, G. A.; Salvador, P.; Dannenberg, J. J.; Zakrzewski, V. G.; Dapprich, S.; Daniels, A. D.; Strain, M. C.; Farkas, O.; Malick, D. K.; Rabuck, A. D.; Raghavachari, K.; Foresman, J. B.; Ortiz, J. V.; Cui, Q.; Baboul, A. G.; Clifford, S.; Cioslowski, J.; Stefanov, B. B.; Liu, G.; Liashenko, A.; Piskorz, P.; Komaromi, I.; Martin, R. L.; Fox, D. J.; Keith, T.; Al-Laham, M. A.; Peng, C. Y.; Nanayakkara, A.; Challacombe, M.; Gill, P. M. W.; Johnson, B.; Chen, W.; Wong, M. W.; Gonzalez, C.; Pople, J. A. *Gaussian 03*, Revision C.01; Gaussian, Inc: Wallingford, CT, 2004.

(58) Stephens, P. J.; Devlin, F. J.; Chabalowski, C. F.; Frisch, M. J. *J. Phys. Chem.* **1994**, *98*, 11623–11627. Hertwig, R.H.; Koch, W. *Chem. Phys. Lett.* **1997**, *268*, 345–351.

(59) Dunning Jr, T. H.; Hay, P. J. *Modern Theoretical Chemistry*; Plenum: New York, 1976; Vol. 3.

(60) Hay, P. J.; Wadt, W. R. *J. Chem. Phys.* **1985**, *82*, 270.

(61) Wadt, W. R.; Hay, P. J. *J. Chem. Phys.* **1985**, *82*, 284.

(62) Hay, P. J.; Wadt, W. R. *J. Chem. Phys.* **1985**, *82*, 299.

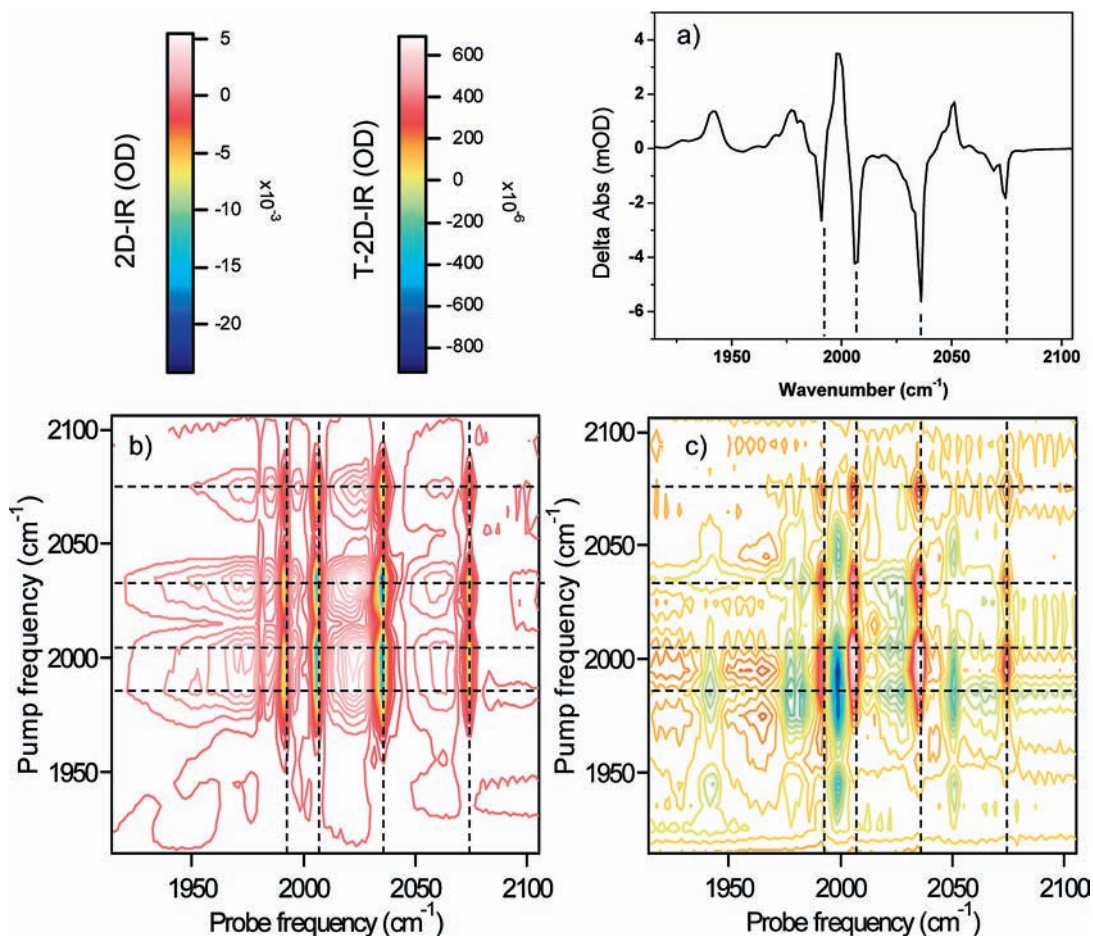


Figure 2. (a) Transient infrared (TRIR; UV_{pump}-IR_{probe}) results for 350 nm photolysis of **1** in heptane with a UV_{pump}-IR_{probe} time delay of 200 ps. (b) 2D-IR (IR_{pump}-IR_{probe}) results for an IR_{pump}-IR_{probe} time delay of 10 ps. (c) T-2D-IR (UV_{pump}-IR_{pump}-IR_{probe}) results with UV_{pump}-IR_{probe} time delay of 200 ps and an IR_{pump}-IR_{probe} time delay of 10 ps. All spectra were recorded during the same experiment, as described in the Experimental Section. The polarization relationships were UV_{pump}:IR_{probe} = parallel; IR_{pump}:IR_{probe} = magic angle. The color schemes (top left) are in units of OD and relate to figures b (2D-IR) and c (T-2D-IR) while the dashed lines are to guide the eye (see text).

using a UV pulse of 350 nm wavelength leads to loss of a carbonyl ligand.¹¹ When performing T-2D-IR studies of this system to gain further insights, there are two time variables that must be considered, that between the IR_{pump} and IR_{probe} and that between the UV_{pump} and IR_{pump} pulses. In the results that follow both of these delays have been varied to extract different sets of dynamical information. In the former case, for a fixed UV_{pump}-IR_{pump} delay time, information relating to the evolution of the infrared excitation is retrieved, yielding vibrational interaction pathways, lifetimes and rotational reorientation times. Information relating to spectral diffusion and chemical exchange may also be obtained.^{36,45,63} Alternatively, fixing the IR_{pump}-IR_{probe} time delay and varying the UV_{pump}-IR_{pump} delay allows access to the evolution of the 2D-IR spectrum as a function of time following the photolysis pulse. In this case, the position of the transitions observed may change if the products evolve with time and structural variation may be observed.

i. Photoproduct 2D-IR Spectroscopy; Fixed UV_{pump}-IR_{pump} Delay Time; Fixed IR_{pump}-IR_{probe} Delay Time. The initial aim of this study was to determine the spectroscopy and number of photoproducts formed upon photolysis of **1**.

Previous TRIR studies show that following photolysis, the infrared spectrum displays a bleach of the ground state vibrational modes of **1**, which recovers on two time scales ~150 ps and ~5 ns. The former was attributed to geminate, or in-cage, recombination while the latter, essentially static, time scale was attributed to slow recovery of the parent molecule following formation of a relatively stable photoproduct.¹¹ In addition to the parent molecule bleaches, a broadband transient absorption, assignable to heating of the system by the photolysis pulse was observed that recovered on a 30 ps time scale. This time scale matched the appearance time of the photoproduct transitions. Thus, to examine the basic spectroscopy of the photoproducts via 2D methods the UV_{pump}-IR_{pump} time delay was set to 200 ps while the IR_{pump}-IR_{probe} time delay was set to 10 ps. The former was chosen to select a dynamically “quiet” regime, as determined by TRIR measurements, in which the photoproducts had formed and were undergoing neither rapid recombination nor vibrational cooling. The latter was selected to be short enough on the time scale of the vibrational lifetime of the photoproducts (see below) to give strong 2D-IR signals while being sufficiently long as to prevent overlap between the IR_{pump} and IR_{probe} pulses, which can result in coherence effects in the spectra. The results of these experiments are shown in Figure 2.

(63) Kwak, K.; Park, S.; Finkelstein, I. J.; Fayer, M. D. *J. Chem. Phys.* 2007, 127, 124503.

Figure 2a shows the TRIR data for this experiment and is simply the $UV_{\text{pump}}-IR_{\text{probe}}$ spectrum obtained with a 200 ps time delay. This shows bleaches corresponding to the four large carbonyl stretching vibrational modes of the parent **1** at 2075, 2035, 2006, and 1991 cm^{-1} ; these are identified by the termini of the four vertical dashed lines in the figure. It is noted that the fifth mode located at 1982 cm^{-1} is also present but is obscured by a broad photoproduct band. These bleaches are accompanied by four clear photoproduct transitions situated at 2051, 1999, 1978, and 1941 cm^{-1} . The mode at 1978 cm^{-1} is significantly broader than the other three and may indicate the presence of more than one absorption in this region. These line positions are in excellent agreement with previous data,¹¹ though absolute frequencies vary by $\pm 2 \text{ cm}^{-1}$ because of the calibration accuracy and resolution ($\sim 4 \text{ cm}^{-1}$) of the spectrometer.

Figure 2b shows the 2D-IR data channel for the measurement. This data is recorded with the UV_{pump} pulse blocked by the chopper and thus corresponds to a double resonance 2D-IR spectrum of the parent molecule recorded with an $IR_{\text{pump}}-IR_{\text{probe}}$ delay time of 10 ps. As a result, this spectrum should contain no contribution from the photoproduct modes observed in Figure 2a. This is indeed the case; the spectrum shows four intense signals on the diagonal corresponding to the line positions of the infrared absorptions of the parent molecule at (probe cm^{-1} , pump cm^{-1}) = (2075, 2075), (2035, 2035), (2006, 2006), and (1991, 1991). Each of these is linked to the other three by off-diagonal peaks indicating vibrational coupling. Corresponding peaks due to the small transition at 1982 cm^{-1} are also observed though are not clearly visible in the 2D representation of the data in Figure 2b. The main peak positions are shown in the figure by horizontal dashed lines. Each of these lineshapes consists of a pair of peaks, one negative, one positive, arising from the $\nu = 0-1$ and $\nu = 1-2$ transitions associated with each mode; the former appears negative because of the bleach of the ground vibrational state caused by the IR_{pump} pulse, while the latter is observed as a positive-going transient absorption. In each case the $\nu = 1-2$ feature is shifted along the probe frequency axis as a result of vibrational anharmonicity and are located at (2067, 2075), (2029, 2035), (2001, 2006), and (1987, 1991). The shifts observed are in good agreement with previous work that showed these values to be mode dependent but that they all lie in the range of 3–6 cm^{-1} .¹⁰ It is also noteworthy that the 2D lineshapes are not diagonally elongated; the nodal plane between the positive and the negative features is parallel to the pump frequency axis in each case. This indicates that any contributions to inhomogeneous broadening of these absorptions arise from processes that are fast on the time scale of the measurement (10 ps). This spectrum has been discussed in significantly more detail elsewhere, the only difference between this and previous measurements is due to the somewhat increased broadening of the lineshapes in the pump-axis direction caused by the broader pump pulse bandwidth arising from the use of a second OPA rather than the pulse shaping arrangement to produce the narrow band pump pulses employed previously.¹⁰ Also noticeable in this spectrum is a slight broadening of the positive features to the low probe frequency side of the line shape. This is likely to be due to small populations of

higher-lying vibrational states such as $\nu = 2$ on account of the slightly higher IR_{pump} powers used to recover good signal-to-noise levels in the T-2D-IR spectra. While power dependence measurements were used to select a pump pulse power that minimized this effect, a very small contribution still remains visible in the spectrum in Figure 2b.

Figure 2c shows the T-2D-IR channel for this measurement. In this case, both the UV_{pump} and the IR_{pump} pulses are present and so contributions to the spectrum are expected from both the parent and the photoproduct molecules. The manner of the measurement ensures that the data is presented as a difference spectrum, in other words it shows the effect on the 2D-IR spectrum of the presence of the UV_{pump} pulse, and thus Figure 2c is the 2D equivalent of the TRIR spectrum shown in Figure 2a. As a result of this it would be expected that signals due to the parent will form a pattern in Figure 2c similar in terms of line position to those in Figure 2b; however, the effect of the UV_{pump} pulse is to bleach these parent molecule absorptions via a reduction in population, and thus the 2D signal following the UV_{pump} pulse will be smaller than that in the absence of this pulse. This effect causes the “phase” of the parent 2D lineshapes to be reversed, by which it is meant that the $\nu = 0-1$ contribution will now be positive-going and the $\nu = 1-2$ contribution will become a negative feature. These can be clearly seen in Figure 2c and are highlighted by the crossing points of the dashed lines, which show the pump and probe frequencies of the parent molecule transitions.

Having thus isolated the 2D “bleaches” from the parent molecule in Figure 2c, any remaining contributions to the spectrum might be expected to be attributable to vibrational modes of the photoproduct. Indeed, several features can be observed in the spectrum that do not coincide with the dashed guide lines. In particular, new modes are visible on the spectrum diagonal at (2050, 2050), (1999, 1999), (1978, 1978), and (1943, 1943). It is noted that the phase of these lines is expected to be the opposite of those due to the parent molecule in Figure 2c as these are new features created by the UV pulse, as such the $\nu = 0-1$ transitions should be negative-going and this is what is observed. In Figure 2c, the accompanying positive features due to the $\nu = 1-2$ transitions are not clearly defined as a result of the large scale of the parent molecule features; these can, however, be seen in cross sections through the data as will be discussed below. It is important to note that the new diagonal peaks occur at frequencies that correspond well with those of the photoproduct bands in the TRIR spectrum of Figure 2a and as such it is reasonable to assign these features to the diagonal modes of the photoproduct spectrum. In addition to these new diagonal modes in Figure 2c, it is possible to discern off-diagonal peaks linking the diagonal peaks discussed above. Specifically, these can be observed in Figure 2c at (2051, 1999), (2051, 1978), (2051, 1943), (1999, 2051), (1999, 1978), (1999, 1943), (1978, 1999), (1978, 1943), (1943, 1999), and (1943, 1978). Closer examination of the data shows that off-diagonal peaks link all of the observed new diagonal modes and suggest that the four photoproduct vibrational modes present in the TRIR spectrum (Figure 2a) are vibrationally coupled and may indicate a single photoproduct species. Some of these peaks are too weak to be observed in Figure 2c but can be seen in

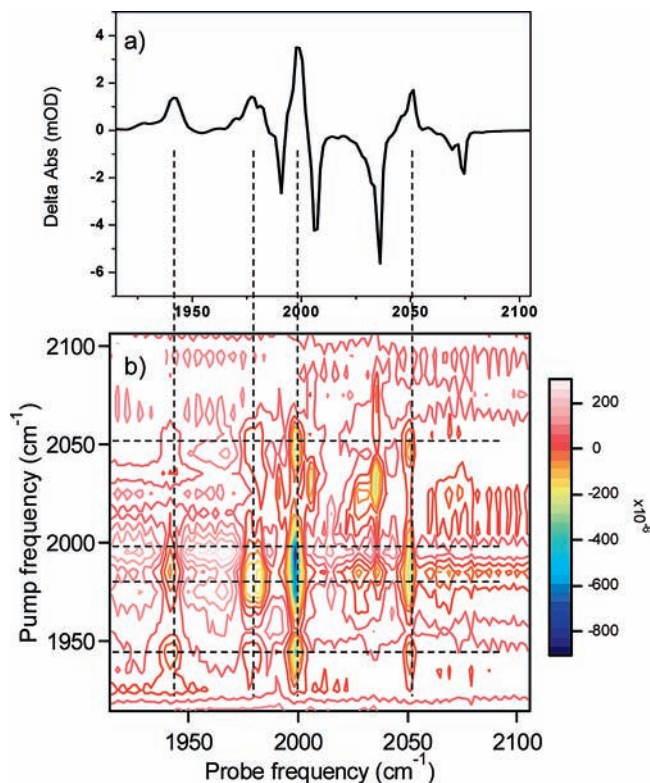


Figure 3. (a) TRIR spectrum repeated from Figure 2a. (b) “Double difference” T-2D-IR spectrum of **1** in heptane solution from which the parent molecule 2D-IR contributions have been subtracted. Dashed lines indicate the positions of 2D-IR lines due to the photoproduct, including off-diagonal features. The color scale for (b) is in units of OD.

cross-section, see below. To emphasize the positions of these new peaks, Figure 3 shows the TRIR spectrum from Figure 2a alongside a “double difference” T-2D-IR spectrum in which the 2D-IR spectrum of the parent molecule (Figure 2b) has been inverted and scaled to match the corresponding features in Figure 2c before being subtracted from the data in Figure 2c leaving the 2D-IR spectrum of the photoproduct only (Figure 3b). This process subtracts the entire 2D-IR contribution of the parent molecule, including peaks due to both $\nu = 0-1$ and $\nu = 1-2$ contributions. The photoproduct peaks are marked in Figure 3b by the intersections of dashed lines, in this case the vertical dashed lines originate from photoproduct bands in the TRIR response, and the good agreement between these and the T-2D-IR diagonal peaks can be seen clearly. The double difference approach is remarkably successful in eliminating the contributions of the parent molecule, despite the relative size of these in comparison to those of the photoproduct. The main artifact of the subtraction process appears to be a residual diagonal peak at (~ 2030 , ~ 2030) which could correspond to a small error in the subtraction of the largest of the parent molecule vibrational modes. This peak also exhibits two small cross-peaks located at $\sim (2030, 2005)$ and $\sim (2005, 2030)$, which are also close to strong parent-mode contributions to the 2D-IR spectrum and again suggest incomplete subtraction. This does not, however, exclude the possibility that the peaks observed are due to the presence of new modes arising from a different photoproduct species that are almost coincident with the parent mode peaks. If this is the case, assignment to

a different species is made on the basis of the lack of vibrational coupling to the main photoproduct peaks described above; however, such an assignment would seem inconclusive from this data, and the remaining discussion will concentrate on the main photoproduct species.

The 2D-IR peaks due to the photoproduct, shown in Figures 2c and 3b, provide information relating to the spectroscopy and dynamics of the species resulting from photolysis of the parent. It is interesting to note that, as well as showing coupling between each of the diagonal photoproduct modes, the 2D-IR lineshapes are all similar in that they show no evidence of the diagonal peak elongation attributable to inhomogeneous broadening with spectral diffusion dynamics that are slow on the experimental time scale (10 ps for the data in Figures 2c and 3b). This is perhaps as would be expected given the anticipated close chemical similarity between parent and photoproduct. Furthermore, examination of the peak shapes show that the separations of the $\nu = 0-1$ and $\nu = 1-2$ components of the lines due to the photoproduct are similar to those of the parent; the anharmonic shifts of the $\nu = 1-2$ components being between 5 and 10 cm^{-1} for each of the diagonal transitions. These are not well resolved in the 2D representations of the data but can be clearly seen in Figure 4, where slices through the T-2D-IR spectra are shown.

Figure 4a shows the 2D-IR response of the parent molecule with a pump frequency of 2075 cm^{-1} for a range of $\text{IR}_{\text{pump}}\text{-IR}_{\text{probe}}$ time delays, while Figure 4b shows the T-2D-IR double difference data for a pump frequency of 1999 cm^{-1} . The differences in the spectra of the parent and photoproduct are clear, as are the presence of the negative ($\nu = 0-1$) and positive ($\nu = 1-2$) components of the photoproduct transitions. The presence of the residual peak near 2030 cm^{-1} is also seen in Figure 4b. The vibrational dynamics of the photoproduct modes will be discussed in more detail below.

ii. Photoproduct Chemistry; Variable $\text{UV}_{\text{pump}}\text{-IR}_{\text{pump}}$ Delay Time; Fixed $\text{IR}_{\text{pump}}\text{-IR}_{\text{probe}}$ Delay Time. Previous TRIR studies of the photolysis of **1** in heptane solution¹¹ showed photochemical dynamics on three main time scales; a 30 ps cooling of the system following excitation that coincided with appearance of the photoproduct species, a 150 ps bleach recovery because of in-cage geminate recombination to reform the parent molecule, and a 5 ns bleach recovery time ascribed to slow loss of the photoproduct. To probe the appearance of the photoproduct bands in more detail, T-2D-IR spectra were recorded for a range of $\text{UV}_{\text{pump}}\text{-IR}_{\text{pump}}$ delay times, with the $\text{IR}_{\text{pump}}\text{-IR}_{\text{probe}}$ time fixed at 10 ps. In all cases the $\text{UV}_{\text{pump}}\text{-IR}_{\text{probe}}$ polarization was parallel, though the rapid rotational relaxation time of the photoproduct, which is shown below to be similar to that of **1** in heptane (17 ps¹⁰) ensures that this will impact the signals observed only at the earliest of $\text{UV}_{\text{pump}}\text{-IR}_{\text{pump}}$ times.²² The difference between the geminate recombination time and rotational relaxation time scales is interesting and suggests a significant role for the solvent cage in restricting motion of the photolysis products. The $\text{IR}_{\text{pump}}\text{-IR}_{\text{probe}}$ polarization was set to the magic angle throughout.

The resulting T-2D-IR spectra were very similar to those shown in Figure 2c in terms of both the position and the shape of the 2D lineshapes obtained. The only

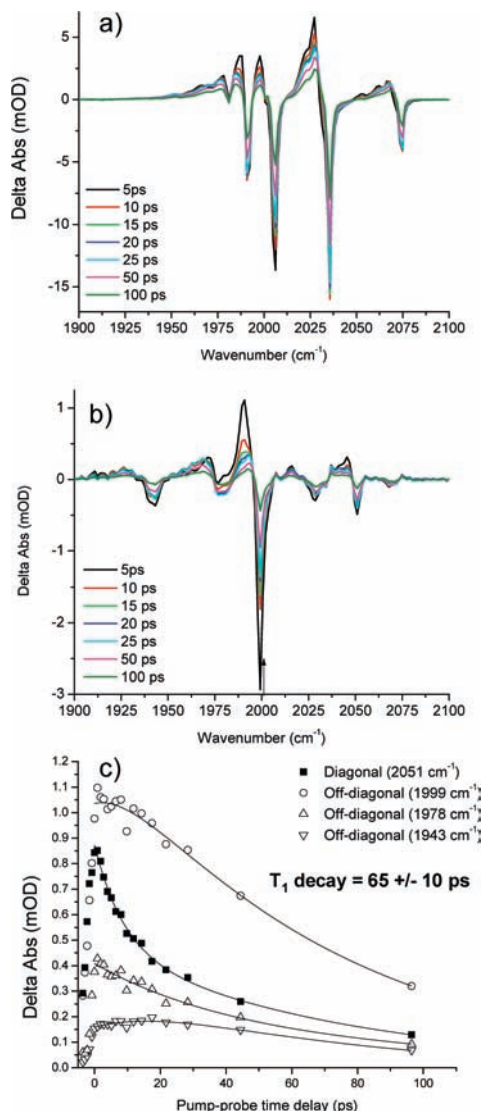


Figure 4. (a) Slice through 2D-IR spectrum of parent molecule recorded with a range of IR_{pump}-IR_{probe} delay times for an IR_{pump} frequency of 2075 cm⁻¹. (b) Slice through T-2D-IR spectrum of photoproduct species recorded with a UV_{pump}-IR_{pump} delay time of 200 ps and a range of IR_{pump}-IR_{probe} delay times for an IR_{pump} frequency of 1999 cm⁻¹, the signal due to the parent molecule has been removed as discussed in the text. (c) Vibrational dynamics observed for the diagonal and off-diagonal photoproduct transitions observed with an IR_{pump} frequency of 2050 cm⁻¹ (IR_{pump}-IR_{probe} polarization: magic angle), solid lines show fits to biexponential functions.

variation observed was a growth of the photoproduct bands and a slight sharpening of the peaks as the vibrational cooling process following photolysis proceeded, as observed via TRIR.¹¹ The new information arises from the relative time scales of appearance for the photoproduct bands on the diagonal and their off-diagonal peaks; it might be expected that if the spectrum were ascribable to a mixture of pentacarbonyl radical and solvent adduct species as was inferred from linear spectroscopy then different peaks and coupling patterns may show different appearance kinetics. Figure 5 shows a summary of the results of these experiments. For clarity, Figure 5a shows slices through the T-2D-IR data at an IR_{pump} frequency of 2075 cm⁻¹, corresponding to the most spectrally isolated vibrational mode of the parent molecule. In this

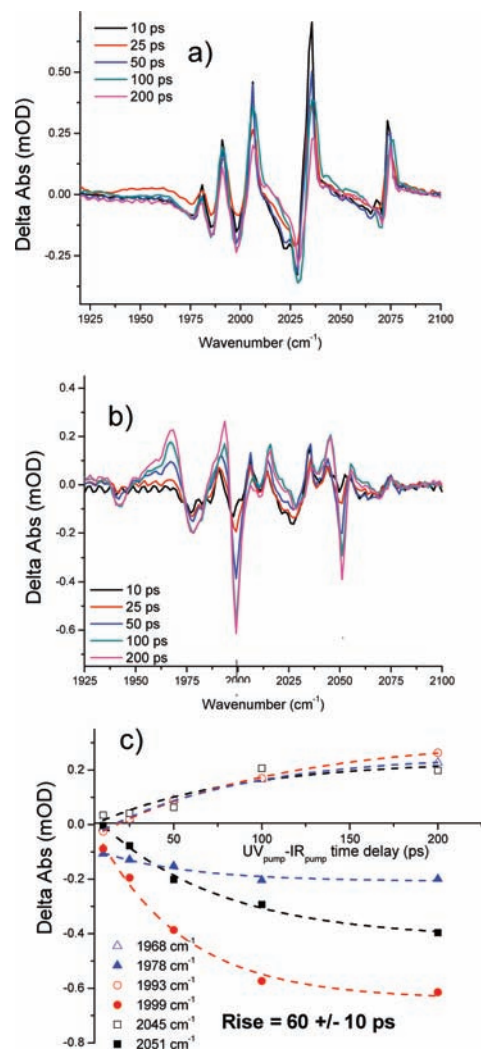


Figure 5. (a) Slice through T-2D-IR spectrum of 1 in heptane with IR_{pump}-IR_{probe} delay time of 10 ps and a variable UV_{pump}-IR_{probe} delay time; the IR_{pump} frequency was 2075 cm⁻¹, coinciding with a bleach of the parent molecule giving rise to an inverted 2D-IR spectrum of 1. (b) Slice through T-2D-IR spectrum of 1 in heptane with IR_{pump}-IR_{probe} delay time of 10 ps and a variable UV_{pump}-IR_{pump} delay time; the IR_{pump} frequency was 2050 cm⁻¹, coinciding with a photoproduct transition. (c) Temporal dependence of photoproduct T-2D-IR peaks; dashed lines show fits to exponential rise functions (see text).

spectrum the inverted 2D-IR response of the parent species is clearly observed, and this data is in excellent agreement with the peak positions (but reversed peak intensities) of Figure 4a as would be expected. Also as expected, these data show a decay profile that broadly matches those observed for the parent bleach recovery in TRIR studies. Figure 5b shows a similar slice through the T-2D-IR data, but at an IR_{pump} frequency of 2050 cm⁻¹, which corresponds to the most isolated photoproduct transition. Again, the peak positions correspond well to those in Figure 4b but the differing intensity ratios of the photoproduct peaks in the two spectra that arise from differing pump frequencies are noted. The presence of a peak at 2020 cm⁻¹ with different dynamics to the photoproduct is noted, though its assignment is unclear. Interrogation of this using 2D-IR methods showed no significant coupling to other modes in this spectral region and as such assignment to a pentacarbonyl species is unlikely.

Table 1. Results of Fitting Data Shown in Fig 4c to Exponential Functions of the Type $\sum A_n \exp(-t/\tau_n)^a$

peak designation	A_R (mOD)	τ_R (ps)	A_1 (mOD)	τ_1 (ps)	A_2 (mOD)	τ_2 (ps)
diagonal (2051 cm^{-1})			0.39	9	0.48	74
off-diagonal (1999 cm^{-1})	0.26	12			1.3	69
off-diagonal (1978 cm^{-1})					0.4	58
off-diagonal (1943 cm^{-1})	0.24	22			0.4	56

^a Subscripts 1 and 2 indicate decay amplitudes (A_n) and time constants (τ_n) for decay processes while the subscript R indicates a rising function.

Figure 5 c shows the temporal dependence of the most intense photoproduct peaks from Figure 5 b, including the $\nu = 1-2$ components as well as the $\nu = 0-1$ transitions. These show the expected rising profile that would be anticipated from TRIR studies and fitting the evolution to an exponential rise function gave time scales of 60 ± 10 ps. The fit results are shown as dashed lines in the figure. This value is slightly greater than those observed via TRIR but with the caveats that T-2D-IR data is of lower signal-to-noise ratio than TRIR signals, the number of data points obtained was fewer than in the TRIR studies because of the time required to obtain T-2D-IR spectra and that the polarization geometry required to extract true photoproduct kinetics is non-trivial in a three-pulse experiment unless the pulse separations are large.²² The lower sensitivity of the T-2D-IR method also means that these peaks correspond to the vibrational ground state of the photoproduct and do not show significant effects due to cooling and the blue shifting due to the presence of higher-lying modes in the manner of TRIR data. The main observation from this data is therefore that the photoproduct peaks show dynamics that are in good agreement with what would be expected, but more crucially, that the diagonal and cross peaks all show the same dynamical trends. This supports the conclusion that the products of photolysis of **1** are singular in nature, though as yet this sheds no light on whether the new species is an unsaturated pentacarbonyl species or a weakly coordinated solvent adduct.

It is interesting to note the very limited effects of vibrational cooling on the T-2D-IR data. The lineshapes observed for the photoproduct species show only a slight narrowing and blue-shifting of both the $\nu = 0-1$ and $\nu = 1-2$ components of the 2D lineshapes (Figure 4b). The number of data points make fitting this process unreliable, and a better measure of this process has been obtained via TRIR data, but the process appears to have been concluded by 50 ps, which is consistent with the cooling rates observed previously.¹¹

Finally, the spectrum in Figure 5b again shows a feature near 2030 cm^{-1} , but it is noted that this feature shows markedly different time dependence to the main bands discussed above. It is assumed that the presence of this mode in this spectral region is due to the overlap of the relatively broad pump pulse spectrum with this peak as consistent coupling patterns between this feature, and the main photoproduct modes were not observed. Efforts to determine the presence of any cross peak patterns from pumping at 2030 cm^{-1} were inconclusive either because of the relatively low signal strength of these features or to spectral overlap with peaks attributable to the main photoproduct species.

iii. Photoproduct Dynamics; Fixed $UV_{\text{pump}}-IR_{\text{pump}}$ Delay Time; Variable $IR_{\text{pump}}-IR_{\text{probe}}$ Delay Time. As mentioned above, the use of a variable $IR_{\text{pump}}-IR_{\text{probe}}$

delay time with a fixed $UV_{\text{pump}}-IR_{\text{pump}}$ delay time allows extraction of vibrational dynamics from T-2D-IR data. The vibrational dynamics of the parent molecule from 2D-IR spectroscopy has been reported elsewhere with intra carbonyl mode vibrational population transfer (IVR) being observed on a time scale of ~ 5 ps, in concert with a T_1 vibrational relaxation time of ~ 120 ps.¹⁰ As the parent molecule data observed via these experiments was in good agreement with that published, this section will concentrate solely on the dynamics of the photoproduct.

The variable $IR_{\text{pump}}-IR_{\text{probe}}$ time delay data was obtained with a fixed $UV_{\text{pump}}-IR_{\text{pump}}$ delay time of 200 ps to separate the effects of population evolution and vibrational dynamics. Further, this delay time ensures the largest photoproduct signals and eliminates the effects of the UV_{pump} pulse polarization on the data because this delay is many times the rotational relaxation time of **1** in heptane solution. The polarization of the IR_{pump} and IR_{probe} pulses was set either to the magic angle, for determination of vibrational relaxation dynamics, or alternately parallel and perpendicular to extract the vibrational anisotropy of the photoproduct modes; it is noted that comparison of the data obtained via the magic angle geometry with the linear combination of parallel and perpendicular responses that mimics the magic angle signal ($R_{\text{para}} + 2R_{\text{perp}}$, where R_x indicates the molecular response under polarization geometry x) showed good agreement.

The nature of the overlapping transitions of parent and photoproduct along with the relatively low signal-to-noise ratios obtained for T-2D-IR data in comparison to that expected for 2D-IR studies made extraction of photoproduct vibrational dynamics somewhat difficult even when employing double difference approaches. The clearest picture was obtained using an IR_{pump} frequency of 2050 cm^{-1} , which coincided with the isolated highest frequency photoproduct mode. The amplitudes of the diagonal and off-diagonal signals corresponding to the $\nu = 0-1$ transitions are shown in Figure 4c as a function of $IR_{\text{pump}}-IR_{\text{probe}}$ delay time. The data in Figure 4c has been fit to exponential functions including rise and decay contributions, and the results are shown in Table 1. The clearest conclusion from the data is that the vibrational relaxation time (T_1) of the photoproduct is on the order of 65 ± 10 ps. A long relaxation component with a similar decay time was obtained consistently from all $\nu = 0-1$ peaks in the T-2D-IR data attributable to the photoproduct species allowing a confident assignment of this value to the T_1 time scale. On shorter time scales, there is some evidence for a second, faster, process that gives rise to a biexponential decay of the diagonal peak at 2051 cm^{-1} and a rise time in two of the three off-diagonal peaks. This would be consistent with the type of intracarbonyl population transfer that has been observed in similar systems.^{9,10} While biexponential decays were consistently observed

for the diagonal photoproduct peaks with a short time scale of the order of the 9 ps reported in Table 1 for the most isolated mode, the extraction of rise times for off-diagonal peaks due to such IVR was heavily dependent on the overlap of the mode in question with other peaks and the relative intensity of the modes; however, the indication of such a process was consistently apparent.

It is interesting to compare the time scales observed for vibrational relaxation in the parent (120 ps¹⁰) and the photoproduct (65 ps). The significantly shorter relaxation time observed for the photoproduct in comparison with that of the parent indicates a significant change in the behavior of the molecule following photolysis, pointing strongly to a solvent adduct species. In a similar study of a metal carbonyl dimer following photolytic cleavage of an intermetallic bond, no change was observed in the vibrational relaxation time between the parent dimer and the product monomer, though a faster intracarbonyl population transfer time was reported.⁵¹ The latter was attributed to a small effect due to slightly increased solvent interaction at a vacant site, though without formation of a solvent adduct. In the case of **1** and its photoproduct, however, the reduced T_1 time scale is evidence of formation of a genuine solvent adduct species. This would promote the long-lived nature of the photoproduct in solution and give rise to an increased solvent interaction capable of facilitating vibrational energy dissipation into the solvent bath.

In light of this increased solvent interaction, it is perhaps surprising that the fast intracarbonyl population transfer time observed for the photoproduct (~9 ps) is apparently longer than that observed for the parent molecule (5 ps¹⁰). Such an effect has been observed however for metal carbonyls solvated by hydrogen-bonding solvents, which increased the level of solvent–solute interaction and promoted vibrational relaxation in comparison to intracarbonyl population transfer (IVR) processes in comparison to polar and aprotic solvents.⁹ It should also be mentioned that the relatively poor determination of this value from the T-2D-IR data may also account for this observation.

Also noteworthy is the comparability of the rise time of the signals due to the photoproduct in the variable UV_{pump}-IR_{pump} delay time experiment and the vibrational relaxation time measured here. The similarity supports the observation that the somewhat limited sensitivity of the T-2D-IR method in comparison to TRIR means that the T-2D-IR spectra observe signals from the vibrational ground state of the photoproduct rather than from any higher-lying levels as the molecules cool following photolysis. Previously reported DFT studies¹¹ indicate that differences in spectral line positions between the unsaturated pentacarbonyl and the solvent adduct should be sufficient to resolve these species, but no changes in photoproduct band position have been observed either via T-2D-IR here or prior TRIR studies,¹¹ indicating that the photoproduct is formed rapidly. While this observation does not indicate whether the photoproduct is an unsaturated pentacarbonyl or a solvent adduct species, the significantly shorter T_1 time is persuasive in support of the latter.

To add weight to the assignment of the observed photoproduct spectral lines to the formation of a solvent

adduct species, DFT calculations have been performed to obtain the structure and predict the infrared spectrum of such a species. The results of this process are shown in Figure 6. The structures shown are the optimized results for the parent species and the two possible solvent adduct species with axial and equatorial substitution of a carbonyl ligand, respectively. It is noted that the propane-dithiolate bridge has been observed to be fluxional on NMR time scales,⁶⁴ but calculations also showed minimal dependence of the infrared spectrum on the position of the apical CH₂ moiety, and for these reasons the second isomer of each compound was not considered further. A propane rather than heptane adduct was used to reduce computational cost; previous work has shown that the length of the carbon chain of the adduct has very little effect on the results of the DFT simulations.¹¹ The spectrum (Figure 6a) shows the predicted infrared absorption of the three molecules in the carbonyl stretching region of the spectrum, to facilitate comparison with experimental data the parent molecule modes have been represented as negative-going features with those of the adducts as positive features. The agreement in terms of spectral pattern is generally good, though the unscaled frequencies appear to underestimate the experimentally observed values, as has been shown to be the case using this method previously.¹⁰ The separation of the two large parent molecule modes near 1980 cm⁻¹ (predicted) is also somewhat smaller than observed, but the ordering of the modes has been shown to be consistent with experiments.¹⁰ It is also clear that identification of the photoproducts on the basis of spectrum alone is not possible using these predictions, given the similarity of the predicted spectral responses, though both bear a close resemblance to the experimental data.

One possible insight into this problem may be possible using the anisotropy data for the photoproduct vibrational modes. When obtaining T-2D-IR data at variable IR_{pump}-IR_{probe} time delays for a fixed UV_{pump}-IR_{pump} time delay of 200 ps using alternating parallel and perpendicular IR_{pump}-IR_{probe} polarization geometry, the linear combination $(R_{\text{para}} - R_{\text{perp}})/R_{\text{magic}}$ yields the anisotropy parameter. The decay of this parameter provides a measure of the molecular reorientation time while the relative values at zero IR_{pump}-IR_{probe} time delay provides the angle between the transition dipole moments of the diagonal and off-diagonal modes. An example of this is shown in Figure 6 b for anisotropy data for the diagonal peak located at 2051 cm⁻¹ and an off-diagonal peak at 1999 cm⁻¹. To account for coherence effects caused by pulse overlap at short times, the data has been extrapolated to zero time via fitting to a single exponential decay function using the assumption that the value for the diagonal peak should be close to 0.4. The decay time scale of the two fits shown are 21 ps for the diagonal peak and 14 ps for the off-diagonal mode, both of which are not inconsistent with the value of 17 ps observed for the parent molecule previously.¹⁰

In the case of Figure 6b, the anisotropy value of ~-0.15 for the off-diagonal mode indicates an angle between the transition dipole moments of ~70 or 110 degrees, though the scatter on the data and the need to extrapolate

(64) Hogarth, G.; Richards, I. *Inorg. Chem. Commun.* **2007**, *10*, 66.

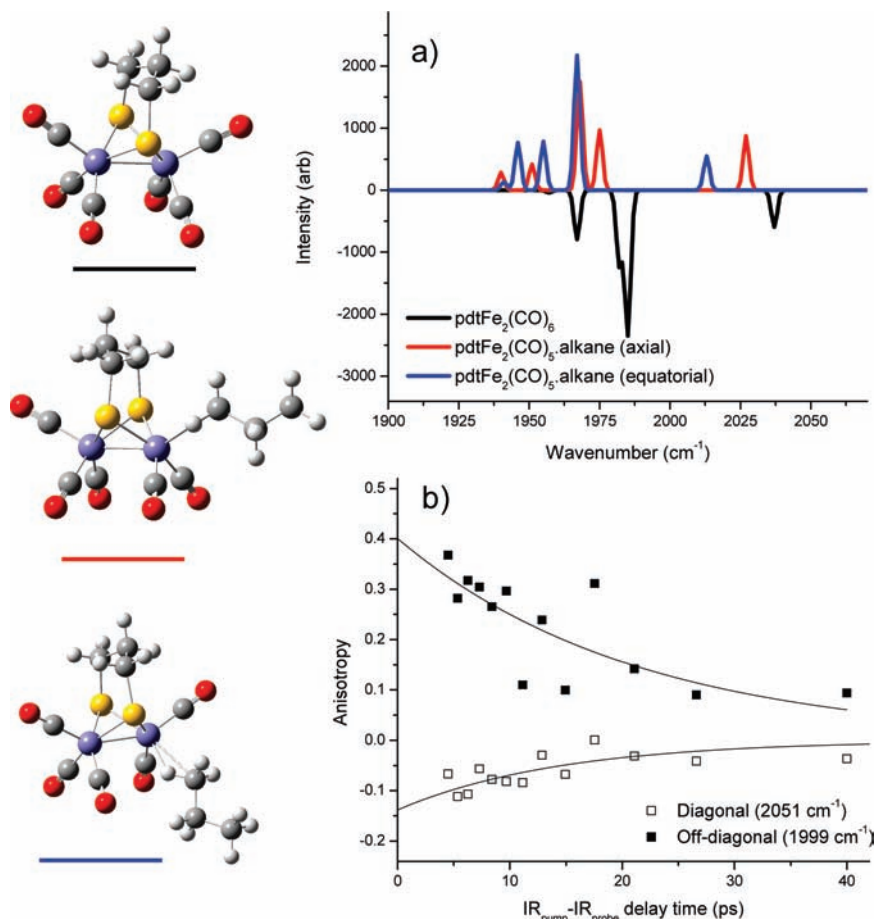


Figure 6. Left, optimized structures for the parent molecule (black) and photoproduct solvent adduct species with axial (red) and equatorial (blue) substitution of a carbonyl ligand for a solvent molecule. Spectrum (a) shows the predicted infrared spectra of these species in the carbonyl stretching region. Trace (b) displays anisotropy data for diagonal (2051 cm^{-1}) and off-diagonal (1999 cm^{-1}) $\nu = 0-1$ components of the T-2D-IR spectrum obtained with a $\text{UV}_{\text{pump}}\text{-IR}_{\text{pump}}$ time delay of 200 ps. The solid line shows a fit to a single exponential decay and the results of extrapolation to zero pump-probe time delay.

to time zero would suggest an error of perhaps ± 15 deg in this value. Repeating this process for the other off-diagonal modes when the IR_{pump} frequency was set to 2050 cm^{-1} indicated the angles between the transition dipole moments for each mode pair to be as shown in Table 2. It is noted first that the mode at 1943 cm^{-1} is excepted from the table on account of the poor signal-to-noise ratio of the anisotropy data for this weak mode and second that the polarization resolved data revealed that the broad mode thus far referred to as 1978 cm^{-1} displayed two components with differing anisotropy, one located at 1978 cm^{-1} and one centered at 1982 cm^{-1} . This is consistent both with the earlier observation that the broad mode may indicate the presence of two transitions and second with DFT calculations that indicate the presence of five carbonyl stretching modes, as would be expected for a pentacarbonyl species lacking significant symmetry. Table 2 also contains the predictions of the angles between transition dipole moments derived from DFT calculations for the axial and equatorial solvent adduct species. The comparisons would seem to tentatively support the formation of the axial adduct species, which would also compare favorably with previous observations that the transition dipole moment for UV excitation leading to photolysis is aligned parallel to the inter-iron bond.¹⁷ It is noted that this analysis requires the assumption that the frequency-ordering of modes calculated

Table 2. Transition Dipole Moment Angles between the Highest Frequency Diagonal Mode and the Associated Diagonal and off-Diagonal Transitions for Experimental Data^a and for DFT Simulations of the Axially and Equatorially Substituted Photoproducts^b

	2051	1999	1982	1978
experiment				
2051	0	110	90	120
DFT axial				
2026	0	90	85	125
DFT equatorial				
2013	0	100	22	120

^a Derived from anisotropy parameters. ^b All frequencies are in cm^{-1} , all angles in deg.

via DFT agrees with those observed experimentally in terms of their assignment. This cannot be independently ascertained, but good agreement between this calculation approach and experiment has been shown in the past for the parent species.¹⁰ Finally, corroboration of the assignment to the axial (or even equatorial) adduct via the other diagonal modes was not possible because of complications arising from overlapping transitions or, in the case of the 1943 cm^{-1} mode, weak spectral features; as a result, we stress that this assignment is tentative. A point worthy of consideration is that the photoproduct species may not be present in a single form; indeed, the DFT predictions suggest that the energy difference between the axial and

the equatorial forms is only 2.6 kJ mol^{-1} in favor of the equatorial form, which might be sufficient to allow interconversion, depending on the activation energy barrier, though it is stressed that no evidence for more than one photoproduct species or indeed interconversion or exchange was observed in the experiments reported herein. It is also noted that the axially substituted photoproduct does not agree with the most energetically probable photoproduct predicted by other recent DFT calculations,¹⁸ though in this case the presence of a solvent molecule was not considered and the relatively similar energies of the two photoproduct structures may complicate the issue. This is clearly an area that will benefit from further study, and it is hoped that the new insight presented here from experiments that are close to the current technical limits of T-2D-IR spectral sensitivity will stimulate discussion and that further technological advances will allow new information to be obtained.

As the weight of evidence would seem to indicate rapid formation of a solvent adduct, this would seem to indicate the sequestration of a solvent molecule from the first solvation shell, which indicates a process following photolysis either of a hot, unsaturated pentacarbonyl undergoing geminate recombination or the formation of a solvent adduct. Predictions of the spectra for the unsaturated species and the solvent adduct suggest sufficient spectral differences that the presence of more than one species, or indeed an electronically excited parent molecule would have yielded complex dynamics for the 2D-IR patterns. The only possible indication of a second species is the feature observed near 2030 cm^{-1} (Figure 3b), while this does display different $UV_{\text{pump}}-IR_{\text{pump}}$ delay temporal dependence to the main photoproduct peaks, it does not show off-diagonal modes remotely consistent with a pentacarbonyl species. The subsequent stability of the main photoproducts alongside the clearly increased vibrational interaction with the solvent therefore strongly suggests the solvent adduct to be the major product. The rapid formation of a solvent adduct species also has implications for any subsequent chemistry of these model species as the resulting adduct would appear to be stable with respect to reformation of the initial species on time scales of ns or greater. This indicates that any further chemistry

will require the presence of a reactant that is able to displace the solvent molecule rather than simply to coordinate with a vacant site, which may limit or at least determine the rate of subsequent mechanistic steps.

Conclusions

In conclusion, we have demonstrated that ultrafast T-2D-IR spectroscopy offers a useful tool for investigating photochemical reactions and have applied it for the first time to study the photolysis products of hydrogenase model compounds. In a significant advance over previous linear infrared spectroscopic studies, T-2D-IR experiments carried out with fixed $UV_{\text{pump}}-IR_{\text{pump}}$ and $IR_{\text{pump}}-IR_{\text{probe}}$ time delays have revealed peaks due to photoproduct species with coupling patterns that are suggestive of a single product. Data obtained using a variable $UV_{\text{pump}}-IR_{\text{pump}}$ time delay have further shown that the peaks due to the photoproduct all exhibit similar dynamics, with no evidence for any short-lived intermediates en route to the formation of the main photoproduct.

Experiments using variable $IR_{\text{pump}}-IR_{\text{probe}}$ delays have been able to determine the vibrational dynamics associated with the photoproduct vibrational modes. These all display a vibrational relaxation time of around 65 ps, significantly shorter than that of the parent, suggestive of a single product species with somewhat greater solvent interactions than the parent. In conjunction with DFT calculations of the infrared spectrum, this information indicates a plausible assignment of the photoproduct spectrum to a solvent adduct species. Finally, analysis of anisotropy data for the peaks observed in the 2D-IR spectrum of the photoproduct indicate a rotational reorientation time scale similar to that of the parent while the derived transition dipole moment angular relationships are more consistent with those calculated for an axial rather than equatorial substitution reaction.

Acknowledgment. The authors acknowledge funding for this work from EPSRC (U.K.) for an Advanced Research Fellowship (N.T.H.) and postgraduate studentship (A.I.S.), from the European Research Council for a Starting Investigator Grant (N.T.H.), and from STFC (U.K.) for a Programme Access Grant (N.T.H.). J.A.W. acknowledges the BBSRC (U.K.) for funding.